
RADIATIVE ASSOCIATION OF AG AND H: FORMATION OF AGH FROM AB INITIO CALCULATIONS *

Lin Jiang, Yu Wang, Xuanbing Qiu, Yali Tian, Guqing Guo, Chuanliang Li

School of Applied Science
Taiyuan University of Science and Technology
Taiyuan

{Yu Wang}wangy@tyust.edu.cn

Yukun Yang

School of Physics
Henan Normal University
Xinxiang

yangyukun@htu.edu.cn

Ling Liu, Yong Wu

Key Laboratory of Computational Physics
Institute of Applied Physics and Computational Mathematics
Beijing

{Yong Wu}wu_yong@iapcm.ac.cn

ABSTRACT

Radiative association processes leading to the formation of AgH in cold astrophysical environments are investigated for the first time using full quantum scattering theory. High accuracy potential energy curves and transition dipole moments for the low-lying electronic states ($X^1\Sigma^+$, $A^1\Sigma^+$, $1^1\Pi$, $3^1\Sigma^+$, $2^1\Pi$) are computed employing the internally contracted multireference configuration interaction method with Davidson correction. Vibrationally and rotationally resolved radiative association cross sections are calculated for transitions from these initial states to the ground $X^1\Sigma^+$ state. Prominent shape resonances arising from quasi-bound rovibrational levels behind centrifugal barriers are identified, with the $2^1\Pi \rightarrow X^1\Sigma^+$ channel exhibiting the strongest contribution at low collision energies. Stimulated radiative association under blackbody radiation fields (up to $T = 20\,000$ K) produces modest enhancements, predominantly in the ground-state channel. Thermal rate coefficients computed over 10^{-1} – 10^4 K reveal a general decreasing trend with temperature for all channels. The results provide essential kinetic data for astrochemical models of transition-metal hydride formation in low-temperature interstellar and circumstellar environments.

Keywords Radiative processes · Reaction rates · Stellar atmospheres

1 Introduction

In astrophysical environments, the formation of molecules is a cornerstone of cosmic chemical evolution. Particularly in low-density regions where three-body collisions are statistically improbable, radiative association (RA)—a process in which two colliding atoms emit a photon to form a bound molecule—serves as the dominant pathway for the genesis of diatomic molecules. For instance, RA plays a crucial role in the synthesis of CH^+ in interstellar clouds, enabling early molecular chemistry in the universe [1], and in forming dust nucleation seeds like MgS in carbon-rich asymptotic giant branch (AGB) stars [2]. Similarly, RA contributes to AlO production in stellar atmospheres, influencing dust grain formation [3].

Driven by its astrophysical significance, the theoretical framework of RA has evolved substantially. Seminal early works laid the foundation: Abgrall et al. (1976) illustrated resonance enhancements in CH^+ formation driven by rotational quantization [1]; Herbst (1980) introduced statistical models affirming RA's efficacy in low-temperature settings [4]; and Bates (1983) synthesized quantum and statistical approaches, offering simplified cross-section formulas [5]. More recent developments have embraced full quantum mechanical computations: Liu et al. (2010) examined competing

**Citation:* Authors. Title. Pages.... DOI:000000/11111.

radiative processes [6]; Stoecklin et al. (2013) refined methodologies for atomic-diatom systems [7]; Babb and colleagues (2017, 2019) computed RA for $C+H^+$ and $C+C^+$ systems, uncovering essential channels and database-ready fitting forms [8, 9]; Šimsová-Zámečnicková et al. (2022) underscored non-adiabatic effects in NaCl [10]; and Chen et al. (2024) supplied data for AlCl and PCl^+ [11]. However, despite this progress, detailed quantum mechanical studies on transition-metal systems remain conspicuously scarce, with Silver Hydride (AgH) being a notable omission.

In the specific case of AgH, existing literature has predominantly focused on its spectroscopic characterization and electronic structure. Learner (1962) furnished spectral constants [12]; Le Roy et al. (2005) captured high-resolution spectra and potential curves for AgH isotopes [13]; Li et al. (2018) pinpointed quasi-closed transitions suitable for laser cooling; Alrebdi et al. (2021) evaluated dipole moments and vibrational levels [14]; Zhou et al. (2023) analyzed spin-orbit coupling influences [15]; and Mohammadian et al. (2024) reclassified excited states while computing Einstein coefficients [16]. Nevertheless, RA processes in AgH have yet to be explored. This oversight is noteworthy, given that silver permeates the interstellar medium via supernova ejecta and AGB star outflows [17], and comparable metal hydrides such as AlH have been observed in stellar atmospheres [18]. Thus, examining RA for AgH offers valuable perspectives on the genesis of transition-metal hydrides in cold astrophysical settings.

2 Method of calculation

2.1 Electronic-structure methodology

The electronic structure calculations for AgH were carried out with the MOLPRO 2012 package [19, 20]. For the Ag atom, the aug-cc-pVTZ-PP basis set was employed together with the Stuttgart ECP28MDF small-core relativistic effective core potential [21], which replaces the 28 inner-shell electrons ($1s^2 2s^2 2p^6 3s^2 3p^6 3d^{10}$) and incorporates scalar relativistic effects. The H atom was described using the all-electron aug-cc-pVTZ basis set. This computational setup is consistent with recent high-level studies on AgH and related spectroscopic properties [15, 16].

All calculations were performed in the C_{2v} point group, the largest Abelian subgroup of $C_{\infty v}$, with the symmetry correspondence $\Sigma^+ = A_1$, $\Pi = B_1 + B_2$, $\Delta = A_1 + A_2$, and $\Sigma^- = A_2$. The molecular orbitals were first generated at the Hartree–Fock level [22], followed by state-averaged CASSCF calculations. The state averaging included five states of A_1 symmetry, two states of B_1 , two states of B_2 , and one state of A_2 . The active space comprised 12 valence electrons distributed in 10 active orbitals, corresponding to the Ag 4d, 5s, 5p, 6s and H 1s, 2s, 2p shells. The Ag 4s4p semicore orbitals were kept doubly occupied as closed orbitals, while the deeper core electrons were represented by the effective core potential. On top of the SA-CASSCF reference, internally contracted MRCI calculations with Davidson correction (+Q) were carried out to recover dynamic correlation.

The PECs were computed over the internuclear range 0.5–10 Å. Transition dipole moments from the excited singlet states to $X^1\Sigma^+$ and the permanent dipole moment of $X^1\Sigma^+$ were evaluated over the same range. For the scattering calculations, the *ab initio* points were interpolated by cubic splines in the intermediate region, extrapolated at short range with an exponential form,

$$V_S(R) = ae^{-bR} + V_{\min}, \quad (1)$$

where a and b are fitting parameters determined from the slope between the first two *ab initio* data points near the minimum, ensuring a physically realistic Born-Mayer-type repulsion. For $R > 10$ Å (long-range), the tail of the PECs was fitted using

$$V_L(R) = \frac{A}{R^6} + \frac{B}{R^8} + \frac{C}{R^{10}}, \quad (2)$$

with coefficients A , B , C obtained by fitting the *ab initio* data in the long-range region. Similarly, TDMs were fitted as

$$\text{TDM}_L(R) = \frac{D}{R^6} + \frac{E}{R^8} + \frac{F}{R^{10}} + x, \quad (3)$$

with coefficients D , E , F obtained by fitting the *ab initio* data in the long-range region after shifting the data to ensure asymptotic decay to zero at large distances. Here, x represents the TDM value at the maximum computed R , relative to zero (asymptotic limit). This form ensures smooth transitions and physically correct van der Waals behavior in neutral systems, where the leading C_6 term dominates, providing smoother extrapolation than forms with additional C_5 terms (as in some literature for charged or polar systems, e.g. [3]).

2.2 Radiative association cross sections and rate coefficients

Radiative association (RA) occurs when two colliding atoms form a quasi-bound complex that stabilizes by emitting a photon. The cross section for spontaneous transitions from an initial electronic state Λ to a final state Λ' is computed

quantum mechanically [23]:

$$\sigma_{\Lambda \rightarrow \Lambda'}^{\text{sp}}(E) = \frac{64\pi^5}{3\hbar^3 c^3} \frac{p_{\Lambda}}{k^2} \sum_{Jv'J'} \nu_{E,v',J'}^3 S_{JJ'} |M_{EJ,v'J'}|^2, \quad (4)$$

where E is the collision energy, k is the wave number, $\nu_{E,v',J'}$ is the transition frequency with $E_{v'J'}$ the bound state energy, $S_{JJ'}$ is the Hönl-London factor (listed in Table 1; 24), and p_{Λ} is the statistical weight:

$$p_{\Lambda} = \frac{(2S' + 1)(2 - \delta_{0,\Lambda})}{(2L_A + 1)(2S_A + 1)(2L_B + 1)(2S_B + 1)}, \quad (5)$$

where $\delta_{0,\Lambda}$ is the Kronecker delta (equal to 1 if $\Lambda = 0$ and 0 otherwise), $L_{A,B}$ and $S_{A,B}$ denoting the orbital and spin angular momenta of the colliding atoms A and B, respectively, and S' the spin multiplicity of the Λ state. The matrix element $M_{EJ,v'J'}$ is given by [25]:

$$M_{EJ,v'J'} = \int_0^{\infty} \phi_J(E, R) D(R) \psi_{v'J'}(R) dR, \quad (6)$$

where $D(R)$ is the transition dipole moment function, $\phi_J(E, R)$ is the energy-normalized continuum radial wavefunction of the initial state, and $\psi_{v'J'}(R)$ is the bound radial wavefunction of the final state.

Table 1: Hönl-London factors for selected transitions.

	${}^1\Sigma^+ \rightarrow {}^1\Sigma^+$	${}^1\Pi \rightarrow {}^1\Sigma^+$
P-branch	J	$(J+1)/4$
Q-branch	–	$(2J+1)/4$
R-branch	$J+1$	$J/4$

To account for stimulated emission induced by a blackbody radiation field at temperature T_b , the partial cross section for each rovibrational transition (v', J') is enhanced by the stimulation factor [26]:

$$\sigma_{\Lambda \rightarrow \Lambda'}(E; T_b) = \frac{\sigma_{\Lambda \rightarrow \Lambda'}^{\text{sp}}(E)}{1 - \exp(-h\nu_{E,v',J'}/k_B T_b)}. \quad (7)$$

The photon occupation number in the blackbody field provides the additional stimulated contribution, which becomes significant at higher radiation temperatures or for transitions with lower frequencies $\nu_{E,v',J'}$. The total cross section is obtained by summing the enhanced partial contributions over all accessible (v', J') levels. When $T_b = 0$ K, the stimulation factor reduces to unity and the expression recovers the pure spontaneous case.

The thermal rate coefficients are obtained by averaging the cross sections over a Maxwell–Boltzmann velocity distribution:

$$k_{\Lambda \rightarrow \Lambda'}(T) = \sqrt{\frac{8}{\mu\pi(k_B T)^3}} \int_0^{\infty} E \sigma_{\Lambda \rightarrow \Lambda'}(E) e^{-E/k_B T} dE, \quad (8)$$

where T is the gas temperature, μ the reduced mass, and k_B the Boltzmann constant.

3 Results and Discussion

3.1 Electronic structure of AgH

The calculated PECs of the five low-lying singlet states, together with the transition dipole moments (TDMs) from the excited states to $X^1\Sigma^+$ and the permanent dipole moment (PDM) of the $X^1\Sigma^+$ ground state, are displayed in Figure 1. The corresponding long-range fitting coefficients of the PECs and dipole moments, as well as the statistical weights p_{Λ} relevant to the radiative association channels, are summarized in Table 2. The calculated asymptotic energies agree well with the NIST values [27, 28, 29], with deviations of 0.034 eV for the $\text{Ag}(4d^{10}5p) + \text{H}(1s)$ limit and 0.045 eV for the $\text{Ag}(4d^9 5s^2) + \text{H}(1s)$ limit, supporting the reliability of the present MRCI+Q treatment.

The $X^1\Sigma^+$ and $A^1\Sigma^+$ states exhibit relatively deep wells, whereas the $1^1\Pi$, $3^1\Sigma^+$, and $2^1\Pi$ states are shallower. This difference is important for the subsequent RA dynamics, since it directly affects the density and character of the quasi-bound levels in the entrance channels. In the dipole-moment curves, the $A^1\Sigma^+ - X^1\Sigma^+$ and $3^1\Sigma^+ - X^1\Sigma^+$ transitions show abrupt changes near 1.8 Å, while the $1^1\Pi - X^1\Sigma^+$ and $2^1\Pi - X^1\Sigma^+$ transitions vary sharply near 1.3 Å. These features are associated with weak avoided crossings in the corresponding excited-state PECs. The PDM of $X^1\Sigma^+$

Table 2: Molecular states of AgH correlating with the lowest dissociation limits, together with the asymptotic energies, long-range fitting coefficients of the PECs and TDMs (PDM for $X^1\Sigma^+$), and the statistical weights p_Λ . All coefficients are in atomic units; numbers in parentheses denote powers of 10.

Asymptotic atomic states	State	NIST (eV)	Molpro (eV)	PEC fitting Coefficient			TDM(PDM) fitting Coefficient			p_Λ
				A	B	C	D	E	F	
Ag($4d^{10}5s^2S$) + H($1s^2S$)	$X^1\Sigma^+$	0.000	0.000	7.617(3)	8.767(1)	-9.687(4)	4.221(1)	-8.411(4)	4.184(7)	1/4
Ag($4d^{10}5p^2P^\circ$) + H($1s^2S$)	$A^1\Sigma^+$	3.664	3.698	2.689(2)	1.832(2)	-2.224(5)	-3.442(2)	5.632(5)	-1.836(8)	1/12
	$1^1\Pi$	3.664	3.696	1.784(1)	-2.176(2)	2.893(4)	1.175(1)	-1.965(4)	6.895(6)	1/6
Ag($4d^95s^2^2D$) + H($1s^2S$)	$3^1\Sigma^+$	3.750	3.795	1.486(1)	-2.002(2)	3.623(4)	-1.590(1)	2.509(4)	-7.466(6)	1/20
	$2^1\Pi$	3.750	3.795	-2.996(2)	1.204(2)	-1.035(5)	1.540(2)	-2.473(5)	7.574(7)	1/10

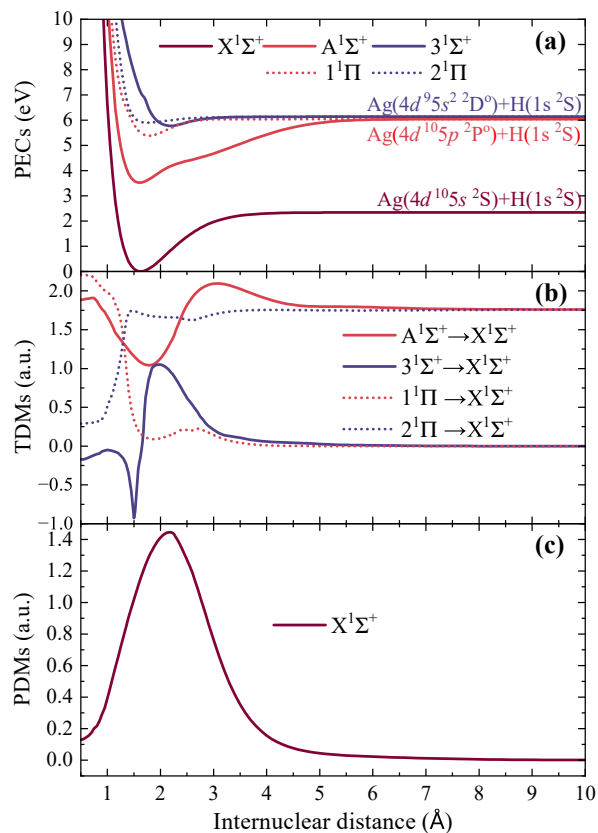


Figure 1: Potential energy curves for the five low-lying $\Lambda - S$ states of AgH, transition dipole moments from excited states to $X^1\Sigma^+$, and permanent dipole moment of the $X^1\Sigma^+$ ground state.

Table 3: Spectroscopic constants of the low-lying electronic states of AgH.

State	R_e (Å)	ω_e (cm ⁻¹)	$\omega_e\chi_e$ (cm ⁻¹)	B_e (cm ⁻¹)	D_e (eV)
X ¹ Σ ⁺	1.62 ^e	1749.58 ^e	35.42 ^e	6.19 ^e	2.34 ^e
	1.61 ^a	1767.47 ^a	36.38 ^a	6.48 ^a	2.36 ^a
	1.62 ^b	1759.90 ^b	34.18 ^b	6.50 ^b	2.38 ^b
A ¹ Σ ⁺	1.60 ^e	1577.78 ^e	53.38 ^e	6.27 ^e	2.52 ^e
	1.62 ^a	1812.19 ^a	63.20 ^a	6.38 ^a	2.36 ^a
	1.64 ^c	1663.60 ^c	87.00 ^c	6.27 ^c	2.36 ^c
1 ¹ Π	1.78 ^e	1480.50 ^e	85.60 ^e	5.49 ^e	0.66 ^e
	1.79 ^d	1477.00 ^d	62.00 ^d	5.28 ^d	0.63 ^d
2 ¹ Π	1.75 ^e	852.00 ^e	90.33 ^e	4.76 ^e	0.24 ^e
3 ¹ Σ ⁺	2.20 ^e	1264.00 ^e	130.77 ^e	3.78 ^e	0.37 ^e

Note. *a:* (author?) [15]; *b:* (author?) [13]; *c:* (author?) [12]; *d:* (author?) [30]; *e:* present work.

increases first and then gradually approaches zero at large R , reflecting the transition from the bonded region to the neutral separated atom limit.

To further assess the quality of the present electronic-structure results, Table 3 compares the calculated spectroscopic constants with available theoretical [15, 30] and experimental [13, 12] data. For the X¹Σ⁺ ground state, the present values of R_e , ω_e , $\omega_e\chi_e$, B_e , and D_e are in good agreement with previous high-level calculations and spectroscopic measurements [15, 13]. The same is true, at least qualitatively, for the excited singlet states, considering that some of them are relatively shallow and more difficult to characterize accurately. The overall agreement is satisfactory, confirming that the present electronic structure results provide a reliable basis for the radiative association calculations discussed below.

3.2 Vibrationally and rotationally resolved cross sections

The radiative association (RA) cross sections for the Ag + H collision system were computed using a full quantum mechanical approach, incorporating the high-precision *ab initio* PECs and TDMs/PDM. As an illustrative example, Figure 2 presents the vibrationally and rotationally resolved cross sections for the ground-state X¹Σ⁺ → X¹Σ⁺ channel, corresponding to spontaneous RA ($T = 0$ K). Panel (a) displays the partial cross sections summed over all vibrational quantum numbers v for fixed rotational quantum numbers J ($J = n$), compared to the total cross section; panel (b) shows the sums over J for fixed v ($v = n$); and panel (c) highlights contributions from specific (v, J) ro-vibrational states. The cross sections exhibit sharp resonances, particularly in the 10⁻⁴–5 × 10⁻¹ eV, arising from quasi-bound states formed behind centrifugal barriers in the effective potential.

Analysis of figure 2 panel (a) reveals that the dominant contributions to the total cross section stem from $J = 9$ –16, with $J = 11$ providing the largest enhancement due to optimal centrifugal barrier effects that trap the colliding partners, promoting resonance formation. Each J contributes resonances across the energy range, but as J increases, the number of resonances diminishes, nearly vanishing by $J = 18$, as the stronger centrifugal repulsion shifts the effective potential, reducing accessible quasi-bound levels at higher energies. Combining this with Figure 2 panel (b), which shows sums over J for fixed v , indicates that these resonances are primarily driven by individual vibrational modes v . Notably, the resonance peaks at specific energy positions are dominated by higher v values, exhibiting a progressive relationship where peak positions shift to higher energies with increasing v . In contrast, the low-energy region (less than 10⁻⁴ eV) is primarily contributed by $v = 0$. Figure 2 panel (c) confirms that specific (v, J) states, such as (5, 11) and (6, 11), account for the major resonances. Notably, as the energy increases, the dominant contributions shift from $J = 11$ to progressively lower values such as $J = 10, 9, 8$, and 7, indicating that lower angular momentum channels become more influential at higher energies; conversely, v gradually increases from 5 to 47, reflecting the accessibility of higher vibrational states at elevated energies. This is consistent with the observations in panels (a) and (b). Physically, this reflects the reduced centrifugal barrier for low- J states at elevated collision energies, allowing easier access to quasi-bound levels and radiative stabilization compared to high- J channels, where the stronger repulsive centrifugal potential suppresses contributions. Furthermore, non-resonant background contributions follow a smooth $E^{-1/2}$ decay, while resonances amplify σ by up to one or two orders of magnitude. These shape resonances enhance the RA efficiency in astrophysical low-temperature environments [31].

Building on the ground-state analysis, the RA cross sections from the excited states (A¹Σ⁺, 1¹Π, 3¹Σ⁺, and 2¹Π) to the ground state at $T = 0$ K (Figure 3) show distinct magnitudes and energy dependences, while all exhibit resonance

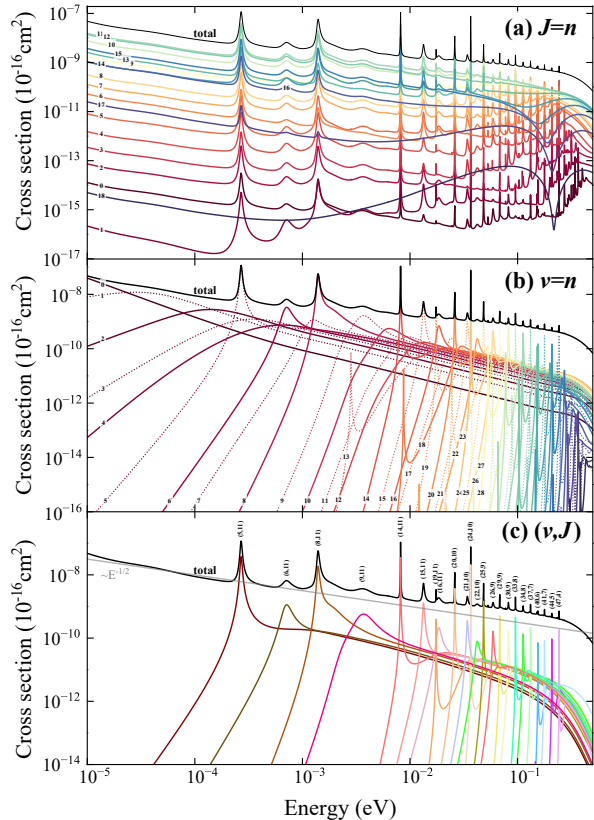


Figure 2: Vibrationally and rotationally resolved radiative association cross sections at $T = 0$ K for the $X^1\Sigma^+ \rightarrow X^1\Sigma^+$ channel in AgH. (a) Partial cross sections summed over vibrational quantum numbers v for fixed rotational quantum numbers J ($J = n$), compared to the total cross section; (b) Partial cross sections summed over J for fixed v ($v = n$); (c) Contributions from specific (v, J) ro-vibrational states, with dominant resonances labeled.

enhancement. The underlying mechanism is similar to that in the ground-state continuum-to-bound process. The main difference arises from the higher dissociation limits of the excited states, which shift the resonance thresholds and modify the Franck–Condon factors. Due to the differing PEC well depths, shallower wells in states like $1^1\Pi$, $3^1\Sigma^+$, and $2^1\Pi$ promote stronger overlap with the incoming continuum wave functions and broader resonances. For instance, the first peak in panel (d) for $2^1\Pi \rightarrow X^1\Sigma^+$ at (2, 8), while the deeper well in $A^1\Sigma^+$ yields more localized quasi-bound states, resulting in narrower features, as seen in the first peak in panel (a) at (4, 14). As energy increases, the resonance peaks gradually narrow, reflecting a faster decay from weak quasi-bound states at high kinetic energies. Each panel shows the total cross section together with the dominant vibrationally and rotationally resolved contributions, labeled by specific (v, J) pairs. As in the ground-state channel, these resonances arise from quasi-bound rovibrational levels supported by the initial-state PECs. Their positions and intensities depend on the electronic-state character and on the associated rovibrational quantum numbers. As collision energy rises, the cross sections from individual ro-vibrational channels gradually diminish, leading to an overall smooth decay in the total RA cross section. These results highlight the pivotal role of the initial electronic state and its ro-vibrational structure in the RA dynamics of AgH, where different electronic states significantly promote molecular formation through quasi-bound ro-vibrational state generation.

3.3 Total cross sections and stimulated radiative association

Figure 4 illustrates the total RA cross sections at $T = 0$ K for AgH formation via radiative transitions from various initial electronic states to the ground state $X^1\Sigma^+$, as a function of collision energy. Notably, the $2^1\Pi \rightarrow X^1\Sigma^+$ channel dominates the overall profile, owing to its favorable TDM and PEC characteristics that enhance continuum-bound overlaps. Resonances manifest in diverse shapes across the channels, reflecting the presence of quasi-bound states supported by the initial electronic effective potentials; these states significantly extend the interaction time of the colliding system, thereby substantially boosting the RA probability. As collision energy increases to around 1 eV, all channels exhibit a rapid decay in RA cross sections, indicating that under high-energy conditions, the system

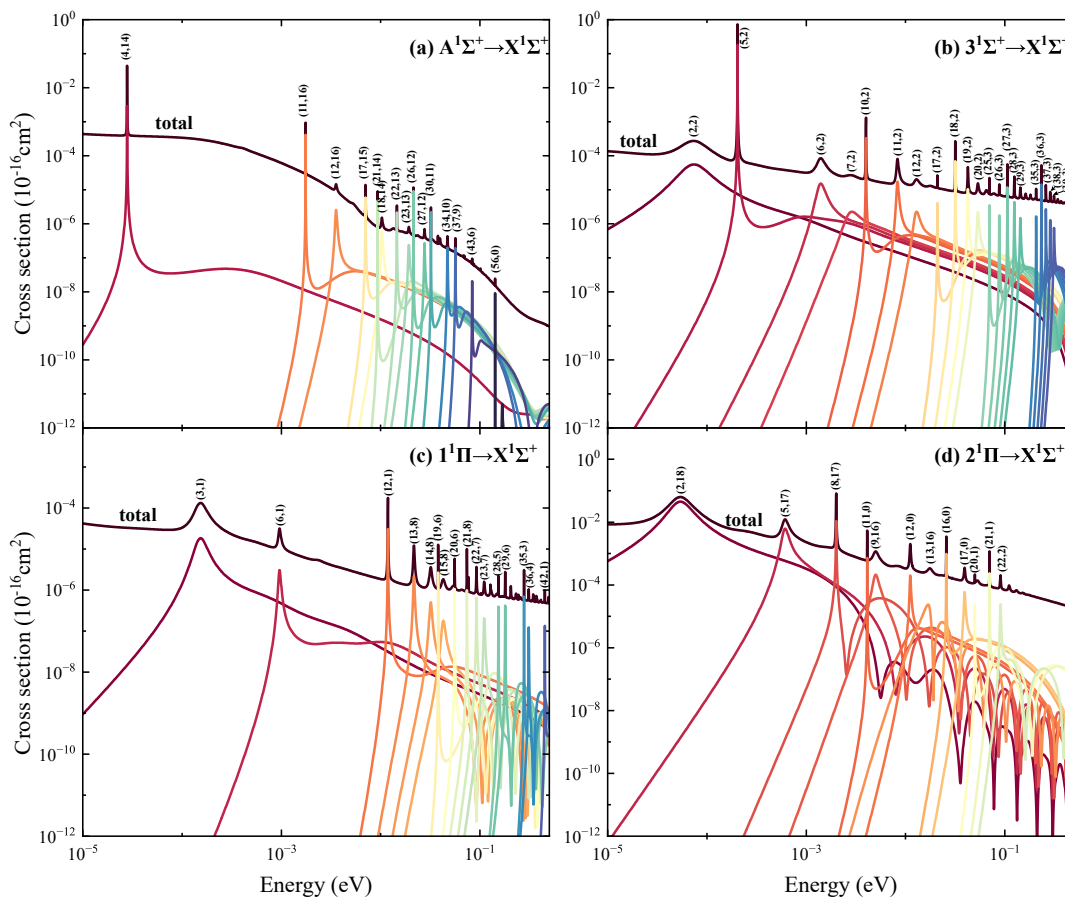


Figure 3: Vibrationally and rotationally resolved radiative association cross sections for transitions from excited states to the ground state $X^1\Sigma^+$ in AgH at $T = 0$ K (spontaneous process).

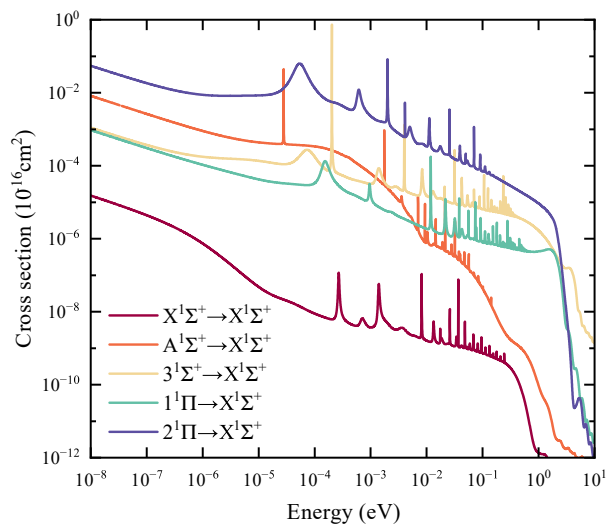


Figure 4: Radiative association cross sections for transitions from the initial states $X^1\Sigma^+$, $A^1\Sigma^+$, $3^1\Sigma^+$, $1^1\Pi$, and $2^1\Pi$ to the ground state $X^1\Sigma^+$ in AgH, calculated at $T = 0$ K.

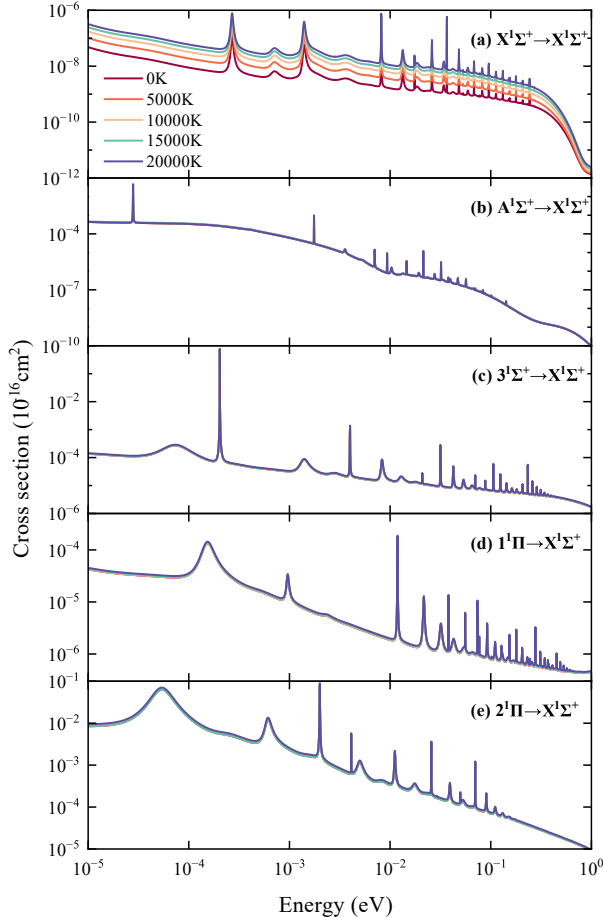


Figure 5: Stimulated radiative association cross sections for AgH formation via transitions from the initial electronic states $X^1\Sigma^+$, $A^1\Sigma^+$, $3^1\Sigma^+$, $1^1\Pi$, and $2^1\Pi$ to the ground state $X^1\Sigma^+$ under blackbody radiation fields with temperatures of 0, 5000, 10000, 15000, and 20000 K.

struggles to effectively dissipate excess kinetic energy via radiative transitions, thus hindering stable molecule formation. Overall, the energy-dependent behavior of AgH’s RA cross sections directly embodies the modulating role of the initial electronic PEC structures on quasi-bound states and resonance effects, providing critical insights into molecular formation kinetics in astrophysical contexts.

To assess the influence of blackbody radiation fields, we computed stimulated RA cross sections for AgH formation from various initial electronic states to the ground state $X^1\Sigma^+$, with radiation temperatures up to 20,000 K. As shown in Figure 5, the overall energy dependence and resonance structures remain essentially unchanged relative to the spontaneous case ($T = 0$ K), indicating that the RA dynamics are primarily governed by the underlying PECs and TDMs.

For the excited-state channels (panels b–e), the cross sections are nearly insensitive to the radiation temperature over the range considered. In contrast, the ground-state channel $X^1\Sigma^+ \rightarrow X^1\Sigma^+$ (panel a) shows a systematic enhancement in magnitude while retaining the same energy profile. The ratios of the stimulated to spontaneous cross sections are approximately 2.12, 3.62, 5.15, and 6.69 at radiation temperatures of 5000, 10000, 15000, and 20000 K, respectively. Thus, blackbody radiation primarily rescales the RA cross sections without altering their intrinsic resonance structures, and its effect is significant only for the ground-state channel.

3.4 Thermal rate coefficients

The thermal rate coefficients for AgH formation via radiative association were obtained by integrating the cross sections over a Maxwell–Boltzmann distribution in the temperature range 10^{-1} – 10^4 K, as shown in Figure 6. The $2^1\Pi \rightarrow X^1\Sigma^+$ channel yields the largest rate coefficient, reaching $\sim 10^{-14}$ $\text{cm}^3 \text{s}^{-1}$ at low temperatures, consistent with its dominant

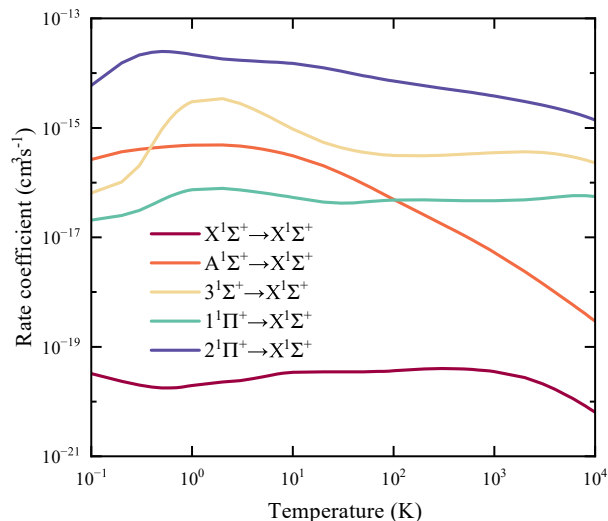


Figure 6: Spontaneous radiative association ($T = 0$ K) rate coefficients for AgH formation via transitions from various initial electronic states to the ground state $X^1\Sigma^+$, as a function of temperature.

cross section. All channels show a general decrease with increasing temperature, reflecting the reduced efficiency of radiative stabilization at higher collision energies.

At low temperatures ($T \leq 10$ K), the rate coefficients are dominated by resonance-rich low-energy cross sections. The $A^1\Sigma^+$ and $3^1\Sigma^+$ channels have comparable magnitudes ($\sim 10^{-16}$ – 10^{-15} $\text{cm}^3 \text{s}^{-1}$), followed by the $1^1\Pi$ channel, whereas the $X^1\Sigma^+ \rightarrow X^1\Sigma^+$ channel remains the weakest. Since the stimulated RA cross sections preserve the same energy dependence as in the spontaneous case (Figure 5), the corresponding thermal rate coefficients at finite radiation temperatures can be obtained by applying multiplicative scaling factors to the $T = 0$ K results. For the excited-state channels, these factors remain close to unity and can be neglected. For the ground-state channel, the rate coefficients are enhanced by factors of 2.12, 3.62, 5.15, and 6.69 at radiation temperatures of 5000, 10000, 15000, and 20000 K, respectively.

At temperatures relevant to circumstellar envelopes and diffuse clouds (~ 10 – 1000 K), the dominant rate coefficients are of the order of 10^{-16} – 10^{-14} $\text{cm}^3 \text{s}^{-1}$, comparable to those reported for analogous species such as AlO [3] and MgS [2], indicating that radiative association is a viable pathway for AgH formation in low-density astrophysical environments. The complete dataset of cross sections and rate coefficients is publicly available at Zenodo (doi:10.5281/zenodo.19041836) for use in astrochemical modeling.

4 Conclusions

Radiative association processes in the Ag + H collision system have been investigated in detail for the first time using full quantum scattering calculations supported by high-accuracy *ab initio* potential energy curves and transition dipole moments for the low-lying electronic states $X^1\Sigma^+$, $A^1\Sigma^+$, $1^1\Pi$, $3^1\Sigma^+$, and $2^1\Pi$. The computed vibrationally and rotationally resolved cross sections reveal prominent shape resonances at ultralow collision energies (10^{-4} – 1 eV), originating from quasi-bound rovibrational levels trapped behind centrifugal barriers in the entrance channels. These resonances significantly enhance association probabilities, with contributions from intermediate rotational quantum numbers ($J \approx 9$ – 16) proving particularly effective in the ground-state channel due to optimal barrier heights that prolong interaction times. Among the examined transitions to the ground $X^1\Sigma^+$ state, the $2^1\Pi \rightarrow X^1\Sigma^+$ channel emerges as the dominant pathway across most of the energy range. Shallower potential wells in states such as $1^1\Pi$, $3^1\Sigma^+$, and $2^1\Pi$ yield broader resonances compared to the deeper $A^1\Sigma^+$ well. Stimulated radiative association under blackbody radiation fields (up to 20 000 K) primarily rescales the cross sections without modifying the intrinsic resonance structures. This effect is significant only for the ground-state $X^1\Sigma^+ \rightarrow X^1\Sigma^+$ channel, whereas the excited-state channels remain nearly unchanged. The thermal rate coefficients, computed over 10^{-1} – 10^4 K, show a general decreasing trend with increasing temperature for all channels, reflecting the decline of RA cross sections at higher collision energies. The dominant $2^1\Pi \rightarrow X^1\Sigma^+$ channel reaches $\sim 10^{-14}$ $\text{cm}^3 \text{s}^{-1}$ at low temperatures, comparable in magnitude to radiative association rates reported for other astrophysically relevant diatomic species such as AlO and MgS. These results address a critical gap in radiative association data for transition-metal hydrides, providing reliable

rate coefficients essential for astrochemical modelling of AgH formation in low-temperature environments, including diffuse interstellar clouds, circumstellar outflows from AGB stars, and cool stellar atmospheres.

Acknowledgments

This work was supported by the National Natural Science Foundation of China (Grant Nos. 12504297, 12304279, 12274040, 62475182), the National Key R&D Program of China (Grant No. 2022YFA1602504), the special fund for Science and Technology Innovation Teams of Shanxi Province (202304051001034), the Special project for science and technology cooperation and exchange of Shanxi Province (202304041101022), the Key Research and Development Program of Shanxi Province of China (202402150301012, 202402130501005, 202302150101006), the Shanxi Province Scientific Research Initial Funding (Grant No. 20252011) and the Taiyuan University of Science and Technology Scientific Research Initial Funding (Grant No. 20242149).

References

- [1] Hervé Abgrall, A. Giusti-suzor, and Èvelyne Roueff. Quantum effects in the formation of ch/plus/ by radiative association. *The Astrophysical Journal*, 207, 1976.
- [2] Wei, Qinghui, Chen, Yang, Xiao, Lidan, Minaev, F. Boris, Ågren, Hans, and Yan, Bing. Radiative association of the magnesium sulfide (mgs) molecule. *A&A*, 699:A264, 2025.
- [3] Gabriella Di Genova, Martina Šimsová née Zámečníková, Lisa Giani, Nadia Balucani, Cecilia Ceccarelli, Marzio Rosi, and Gunnar Nyman. Radiative association formation of alo, a candidate seed of dust nucleation. *Monthly Notices of the Royal Astronomical Society*, 544(3):2860–2869, 10 2025.
- [4] E. Herbst. A new look at radiative association in dense interstellar clouds. *apj*, 237:462–470, apr 1980.
- [5] D. R. Bates. Theory of molecular formation by radiative association in interstellar clouds. *apj*, 270:564–577, jul 1983.
- [6] XJ Liu, YZ Qu, BJ Xiao, CH Liu, Y Zhou, JG Wang, and RJ Buenker. Radiative charge transfer and radiative association in he++ ne collisions. *Physical Review A—Atomic, Molecular, and Optical Physics*, 81(2):022717, 2010.
- [7] T Stoecklin, F Lique, and M Hochlaf. A new theoretical method for calculating the radiative association cross section of a triatomic molecule: application to n 2–h-. *Physical Chemistry Chemical Physics*, 15(33):13818–13825, 2013.
- [8] James F Babb and Brendan M McLaughlin. Radiative association of c (3p) and h+: triplet states. *Monthly Notices of the Royal Astronomical Society*, 468(2):2052–2057, 2017.
- [9] James F Babb, RT Smyth, and BM McLaughlin. Radiative association of atomic and ionic carbon. *The Astrophysical Journal*, 884(2):155, 2019.
- [10] M Šimsová-Zámečníková, P Soldán, and Magnus Gustafsson. Formation of nacl by radiative association in interstellar environments. *Astronomy & Astrophysics*, 664:A5, 2022.
- [11] Yang Chen, Xiaohe Lin, Lidan Xiao, Zijian Li, Songbin Zhang, Yongjun Cheng, Yong Wu, Amaury A de Almeida, Carmen M Andrezza, and Bing Yan. Radiative association for the formation of phosphorus monochloryl cation (pcl+) and aluminium monochloride (alcl). *Monthly Notices of the Royal Astronomical Society*, 533(3):3246–3254, 2024.
- [12] RCM Learner. The influence of vibration-rotation interaction on intensities in the electronic spectra of diatomic molecules ii. the silver hydride molecule. *Proceedings of the Royal Society of London. Series A. Mathematical and Physical Sciences*, 269(1338):327–337, 1962.
- [13] Robert J Le Roy, Dominique RT Appadoo, Kevin Anderson, Alireza Shayesteh, Iouli E Gordon, and Peter F Bernath. Direct-potential-fit analysis of new infrared and uv/visible $a\sigma+ 1-x\sigma+ 1$ emission spectra of agh and agd. *The Journal of chemical physics*, 123(20), 2005.
- [14] Tahani A Alrebdi, Hanen Souissi, Fatemah H Alkallas, and Fatma Aouaini. Ab initio adiabatic study of the agh system. *Scientific Reports*, 11(1):8277, 2021.
- [15] Weiqi Zhou, Yujie Zhao, Guqing Guo, Xiaohu He, Ting Gong, Xuanbing Qiu, Yali Tian, Xiaochong Sun, Shuping Liu, Jianghui Cai, et al. Theoretical study of low-lying electronic states of agh including spin-orbit coupling. *Journal of Molecular Structure*, 1286:135524, 2023.

- [16] Zeinab Mohammadian, Farnoush Nourigheimasi, Ali Maghari, and Alireza Shayesteh. Spin-orbit coupling in excited electronic states of agh. *Chemical Physics Letters*, 849:141418, 2024.
- [17] Edward B. Jenkins. A unified representation of gas-phase element depletions in the interstellar medium*. *The Astrophysical Journal*, 700(2):1299, jul 2009.
- [18] Ian U. Roederer, George W. Preston, Ian B. Thompson, Stephen A. Sheckman, Christopher Sneden, Gregory S. Burley, and Daniel D. Kelson. A search for stars of very low metal abundance. vi. detailed abundances of 313 metal-poor stars*. *The Astronomical Journal*, 147(6):136, may 2014.
- [19] Hans-Joachim Werner and Peter J Knowles. An efficient internally contracted multiconfiguration–reference configuration interaction method. *The Journal of chemical physics*, 89(9):5803–5814, 1988.
- [20] Hans-Joachim Werner, Peter J Knowles, Gerald Knizia, Frederick R Manby, and Martin Schütz. Molpro: a general-purpose quantum chemistry program package. *Wiley Interdisciplinary Reviews: Computational Molecular Science*, 2(2):242–253, 2012.
- [21] Kirk A Peterson. Systematically convergent basis sets with relativistic pseudopotentials. i. correlation consistent basis sets for the post-d group 13–15 elements. *The Journal of chemical physics*, 119(21):11099–11112, 2003.
- [22] Hans-Joachim Werner and Wilfried Meyer. A quadratically convergent multiconfiguration–self-consistent field method with simultaneous optimization of orbitals and ci coefficients. *The Journal of Chemical Physics*, 73(5):2342–2356, 1980.
- [23] B Zygelman and A Dalgarno. The radiative association of he (+) and h. *Astrophysical Journal, Part 1 (ISSN 0004-637X)*, vol. 365, Dec. 10, 1990, p. 239, 240. Research supported by DOE., 365:239, 1990.
- [24] FA Gianturco and P Gori Giorgi. Radiative association of lih ($x 1 \sigma+$) from electronically excited lithium atoms. *Physical Review A*, 54(5):4073, 1996.
- [25] Bernard R Johnson. New numerical methods applied to solving the one-dimensional eigenvalue problem. Technical report, 1977.
- [26] P. C. Stancil and A. Dalgarno. Stimulated Radiative Association of Li and H in the Early Universe. *The Astrophysical Journal*, 479(2):543, April 1997.
- [27] Charlotte Emma Moore. *Atomic energy levels as derived from the analyses of optical spectra*, volume 1. 1949.
- [28] T Badr, MD Plimmer, P Juncar, ME Himbert, JD Silver, and GD Rovera. Continuous-wave doppler-free two-photon spectroscopy of the sd transition in atomic silver. *The European Physical Journal D-Atomic, Molecular, Optical and Plasma Physics*, 31(1):3–10, 2004.
- [29] Thomas Badr, Mark David Plimmer, Patrick Juncar, ME Himbert, Yann Louyer, and DJE Knight. Observation by two-photon laser spectroscopy of the $4 d 10 5 s s 1/2 2 \rightarrow 4 d 9 5 s 2 d 5/2 2$ clock transition in atomic silver. *Physical Review A—Atomic, Molecular, and Optical Physics*, 74(6):062509, 2006.
- [30] Chuanliang Li, Yachao Li, Zhonghua Ji, Xuanbing Qiu, Yunzhong Lai, Jilin Wei, Yanting Zhao, Lunhua Deng, Yangqin Chen, and Jinjun Liu. Candidates for direct laser cooling of diatomic molecules with the simplest $\sigma 1-\sigma 1$ electronic system. *Physical Review A*, 97(6):062501, 2018.
- [31] B. Zygelman, P. C. Stancil, and A. Dalgarno. Stimulated Radiative Association of He and H+. *The Astrophysical Journal*, 508(1):151, November 1998.